

CHARACTERISTICS OF PURE LOVE MODE SAW SENSOR WITH GRAPHENE INTERDIGITAL TRANSDUCER FOR BIOSENSING APPLICATIONS

CHEN CHEN

*Yunnan Key Laboratory of Optoelectronic Information Technology, Yunnan Normal University, Kunming, China
e-mail: chen_chen_1982@163.com*

XINYU WANG, YUTING WANG

Changchun University of Science and Technology, Changchun, Jilin, China

The characteristics of Love wave biosensors are systematically investigated. The results show that sensors with combination of a ZnO guiding layer and 90ST or 90AT Quartz substrates exhibit purer Love modes than those with the SiO₂ guiding layer. The corresponding maximum sensitivities are -10.9069 and -11.641 m²/kg, respectively, which are nearly two times higher than those of SiO₂ layer. The ZnO/90ST Quartz Love wave sensor exhibits the largest K^2 of 0.3022 and achieves 0 ppm/°C of TCF at $h_{\text{ZnO}}/\lambda = 0.0216$. The sensor employing the graphene IDT further improves the sensitivity by nearly one order of magnitude.

Keywords: SAW biosensor, Love mode, graphene, mass sensitivity

1. Introduction

Biosensors (Jandas *et al.*, 2020) are analytical devices used for detection of analytes. They combine biologically sensitive elements called bioreceptors with physicochemical transducers. These bioreceptors are biological materials that can directly bind to target analytes in a sample mixture including tissues, cells, enzymes, antibodies, and nucleic acids. Based on the type of transducers, biosensors can be classified as electrochemical, optical, gravimetric and piezoelectric biosensors (Fan and Ji, 2018; Tang *et al.*, 2019; Turner, 2013).

Surface acoustic wave (SAW) piezoelectric biosensors are one of the most promising sensing platforms because they are highly sensitive to surface perturbations, can operate in both dry and aqueous environments, have wireless operation capability and can be easily fabricated by standard microfabrication techniques. A Love (or SH) mode SAW with only one component of mechanical displacement parallel to the substrate surface and perpendicular to the propagation direction provides low damping in a liquid (Luo *et al.*, 2017a,b). A Love SAW can be generated in a layered structure consisting of a substrate and a waveguide layer when the acoustic velocity of the waveguide layer is lower than that of the substrate. Due to the waveguide effect, most of the wave energy is confined to the waveguide layer. Therefore, the Love wave device is very sensitive to the surface perturbation and is suitable for sensor applications especially in liquids (Luo *et al.*, 2017b; Moreira *et al.*, 2007).

When choosing the substrate material, the SH polarization, which is required for operation of the Love wave sensor in liquid media, should be considered. In this sense, quartz is the only common substrate material that can be used to obtain a purely shear polarized wave (Jakoby *et al.*, 2000). Possible cuts which generate purely shear polarized waves are the AT-cut quartz and the ST-cut quartz. Among the commonly used guiding layers, such as polymethyl-methacrylate (PMMA), SiO₂, and ZnO (Tang *et al.*, 2014; Zadeh *et al.*, 2002), SiO₂ is appropriate for a Love wave biosensor, mainly due to its low damping and excellent chemical and mechanical properties

(Franssila, 2004); ZnO is bio-safe and shows a high affinity for binding biomolecules, making it suitable for biomedical applications to immobilize and modify the biomolecular material without toxic effects (Luo *et al.*, 2013; Fu *et al.*, 2010); however, PMMA has high acoustic damping (Matatagui *et al.*, 2011).

In this paper, characteristics of a Love wave sensor, including phase velocity, electromechanical coupling coefficient, temperature coefficient of frequency, and mass loading sensitivity, based on SiO₂ or ZnO guiding layers overlaid on quartz are systematically investigated. Possible cuts of quartz which generate a purely shear polarized wave are presented.

2. Theory

2.1. Phase velocity

The configuration of the Love-mode waveguide is shown in Fig. 1. The semi-infinite substrate is overlaid by a guiding layer of thickness h . The Love wave propagates in the z direction, and the Love wave shear mechanical displacement is along the x axis. The distributions of the displacements in the x axis (normalized to the values at the surface $y = 0$) can be given by Wang *et al.* (1994)

$$\begin{aligned}\eta_{(y)}^{(1)} &= \cos(\beta_1 h) e^{-\beta_1(y-h)} & y \geq h \\ \eta_{(y)}^{(2)} &= \cos(\beta_2 y) & 0 \leq y \leq h\end{aligned}\quad (2.1)$$

where β_1 is the decay constant in the substrate, β_2 is the transverse propagation constant in the waveguide layer

$$\beta_1 = \sqrt{\frac{\omega^2}{V^2} - \frac{\omega^2}{V_{s1}^2}} \quad \beta_2 = \sqrt{\frac{\omega^2}{V_{s2}^2} - \frac{\omega^2}{V^2}}$$

and ω is the radian frequency, V is the phase velocity, V_{s2} and V_{s1} are the bulk shear velocities of waveguide layer and substrate, respectively.

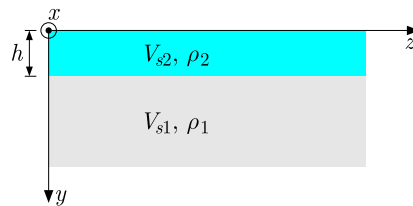


Fig. 1. Configuration of the Love-mode waveguide

For an anisotropic layer of thickness h with constants L_2 and N_2 over an anisotropic semi-infinite substrate with constants L_1 and N_1 , the Love wave equation is given by Anderson (1961)

$$\tan kh \sqrt{\frac{V^2}{V_{s2}^2} - 1} \sqrt{\frac{N_2}{L_2}} = \sqrt{\frac{L_1 N_1}{L_2 N_2}} \sqrt{\frac{1 - \frac{V^2}{V_{s1}^2}}{\frac{V^2}{V_{s2}^2} - 1}} \quad (2.2)$$

where $N_i = (c_{11} - c_{12})/2$, $L_i = c_{44}$ (for substrate $i = 1$, for waveguide layer $i = 2$).

For sensor applications, both β_1 and β_2 should be real, so we only consider the case of $V_{s2} \leq V \leq V_{s1}$.

2.2. Electromechanical coupling coefficient (K^2)

K^2 is a measure of the efficiency of a given SAW device in converting an applied electrical signal into mechanical energy and can be evaluated from the well-known equation

$$K^2 \cong 2 \frac{V_0 - V_s}{V_0} \quad (2.3)$$

where V_0 and V_s are the Love wave velocities calculated for free and electrically shorted surfaces, respectively.

2.3. Temperature coefficient of frequency (TCF)

The TCF is calculated by the equation

$$\text{TCF} = \frac{1}{35 - 15} \frac{V_{35} - V_{15}}{V_{25}} \quad (2.4)$$

where V_{35} , V_{25} , and V_{15} are the phase velocities at 35°C, 25°C, and 15°C, respectively. The temperature dependence of the material constants is approximated by a second-order function, and is given by

$$X = X_0[1 + a_1(T - T_0) + a_2(T - T_0)^2] \quad (2.5)$$

where X_0 is the material constant at room temperature, X is the material constant at any temperature, T_0 is the room temperature, T is temperature, a_1 and a_2 are the first- and second-order temperature coefficients of the material constants, respectively.

2.4. Mass loading sensitivity

The mass loading sensitivity for the acoustic sensor is defined as a relative change of the oscillation frequency due to the mass loading on the surface (Krishnamoorthy and Iliadis, 2008; Powell *et al.*, 2004)

$$S_m^f = \frac{1}{f_0} \lim_{\Delta m \rightarrow 0} \frac{\Delta f}{\Delta m} \quad (2.6)$$

where f_0 is the operational frequency without a perturbation, f is the operational frequency after the perturbation and $\Delta f (= f - f_0)$ is the frequency change due to the mass per unit area Δm deposited on the surface.

3. Results and discussions

3.1. The effect of crystal cut on the shear component of SAWs

The finite element method (FEM) is used to evaluate characteristics of Love wave sensors. In the simulation, the device wavelength λ is selected to be 40 μm , the thickness of substrate is assumed to be 6λ , and the thickness of the guiding layer is 2 μm . Figure 2 shows the displacement components along x , y and z directions as a function of depth y in different combinations of substrates (ST/AT Quartz, 90ST/90AT Quartz) and guiding layers (ZnO, SiO₂). The obtained displacement components rapidly decrease beneath the top surface. For the ST/AT Quartz substrate, Figs. 2a-2d demonstrate the dominant x (out of plane) component whereas the other two components are relatively smaller. For the 90ST/90AT Quartz substrate, Figs. 2e-2h show that no y (depth) and z (propagation) displacement components can be observed and only the x

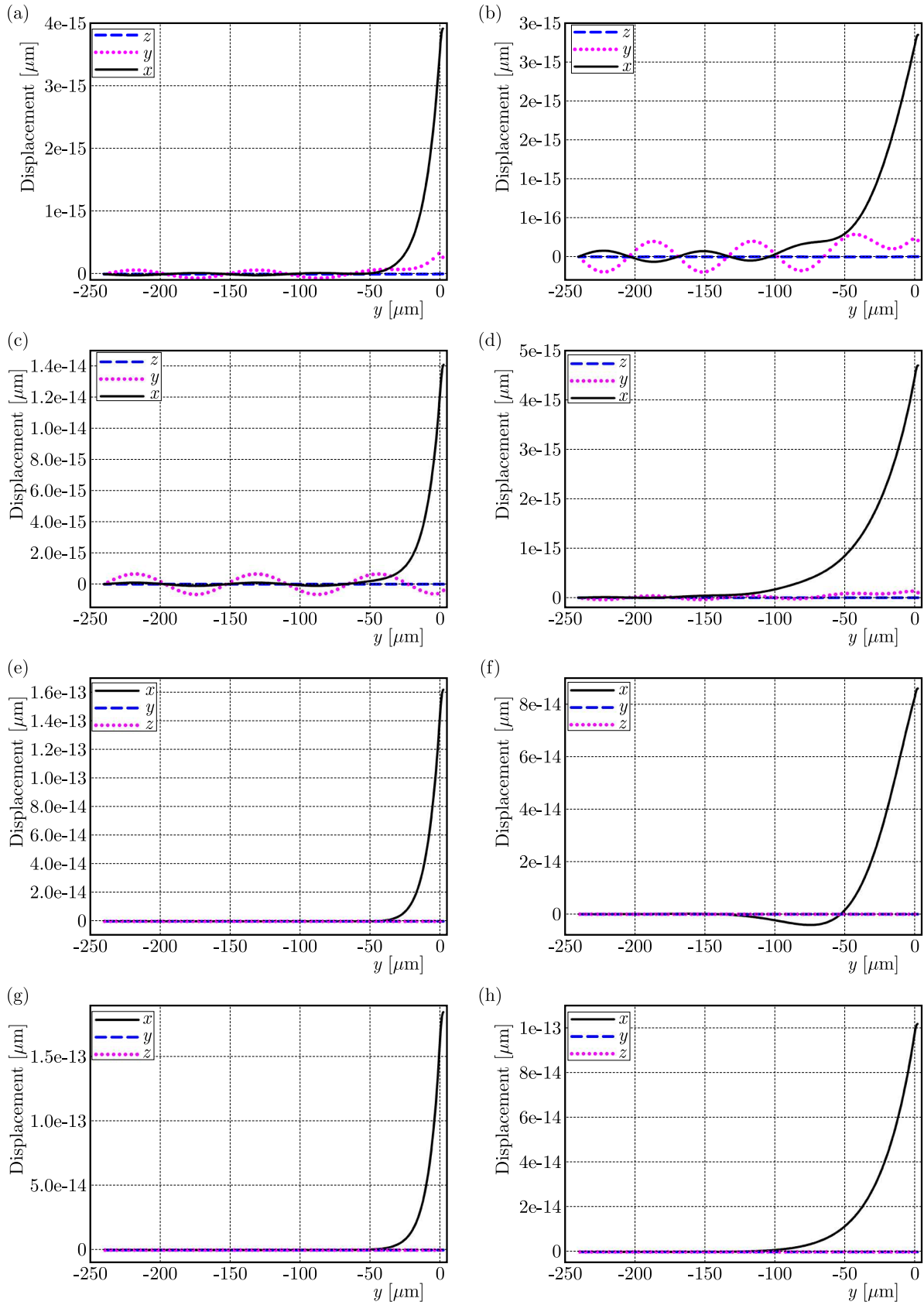


Fig. 2. Displacement components as a function of depth y : (a) ZnO/ST Quartz, (b) SiO₂/ST Quartz, (c) ZnO/AT Quartz, (d) SiO₂/AT Quartz, (e) ZnO/90ST Quartz, (f) SiO₂/90ST Quartz, (g) ZnO/90AT Quartz, (h) SiO₂/90AT Quartz

(out of plane) component can be found, which indicates that the excited SAW is the Love wave. ZnO is more efficient than SiO₂ in converting the bulk SH mode to the Love mode due to its lower shear bulk velocity. The results confirm that the device with the 90ST/90AT Quartz substrate exhibits a purer Love mode than that with the ST/AT Quartz substrate. So, the 90ST and 90AT Quartz substrates are chosen for further research in the following.

3.2. Phase velocity V_p and group velocity V_g

The changes in the phase velocity and group velocity calculated by

$$V_g = V_p \left(1 + \frac{h/\lambda}{V_p} \frac{dV_p}{d(h/\lambda)} \right)$$

as a function of ZnO or SiO₂ normalized thicknesses h/λ are shown in Fig. 3. We are interested in the fundamental Love mode. The phase velocity decreases with the increasing guiding thicknesses. The decrease of V_p with an increase in the normalized guiding thicknesses is due to smaller velocities of ZnO (2720 m/s) and SiO₂ (2850 m/s) than those of the 90ST (5050 m/s) or 90AT (5099 m/s) Quartz substrate. If ZnO and SiO₂ thicknesses get thicker $> \lambda$, the SAW phase velocity will be almost regardless of the 90ST or 90AT Quartz substrate velocity and approach to the shear wave velocities of ZnO and SiO₂. Because of the smaller shear wave velocity of ZnO, the values of V_p exhibit a larger dispersion as a function of h_{ZnO}/λ than those as a function of h_{SiO_2}/λ .

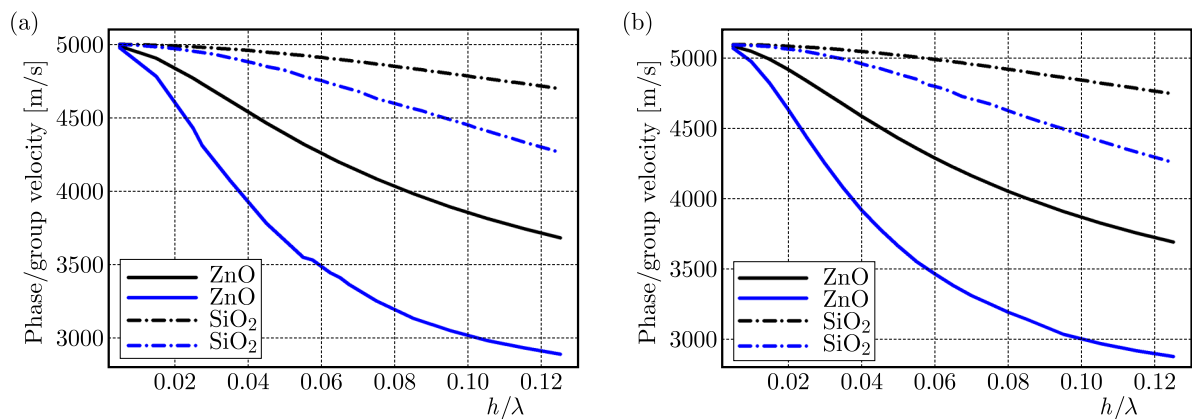


Fig. 3. Velocity dispersions of the Love mode as a function of the normalized guiding layers thicknesses (black line: phase velocity; blue line: group velocity): (a) 90ST Quartz, (b) 90AT Quartz

3.3. Electromechanical coupling coefficient (K^2)

The electromechanical coupling coefficient as a function of ZnO or SiO₂ normalized guiding thicknesses h/λ is shown in Fig. 4 for different substrates (ST/AT Quartz, 90ST/90AT Quartz). It shows that the value of K^2 increases with the increasing normalized thickness and slows down afterwards. Because of the piezoelectricity of ZnO, K^2 increases more rapidly than that of SiO₂ and reaches a larger maximum value at the thinner thickness. Table 1 shows that the ZnO/90ST Quartz and ZnO/90AT Quartz reach the maxima of K^2 at the same ZnO thickness. The ZnO/90ST Quartz structure exhibits the largest K^2 of 0.3022.

3.4. Temperature coefficient of frequency (TCF)

The temperature stability of the frequency in a SAW device is of great importance for sensing application. The TCF close to 0 is expected for many SAW device applications such as sensors

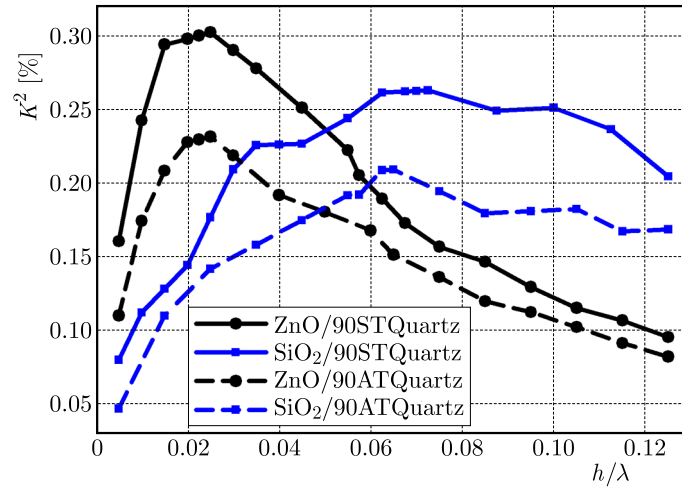


Fig. 4. K^2 dispersion patterns of the Love mode as a function of normalized guiding thickness

Table 1. The maximum of K^2 and its corresponding guiding thickness

Substrate	Guiding layer	K_{max}^2 [%]	h/λ
90ST Quartz	ZnO	0.3022	0.0250
	SiO ₂	0.2629	0.0725
90AT Quartz	ZnO	0.2314	0.0250
	SiO ₂	0.2091	0.0650

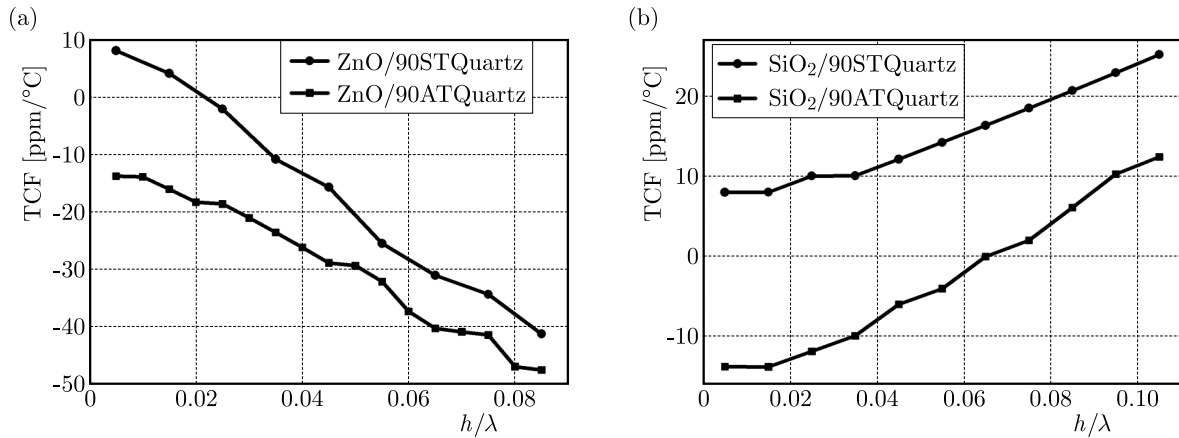


Fig. 5. TCF versus normalized guiding thickness for the Love wave sensor: (a) ZnO guiding layer, (b) SiO₂ guiding layer

and wireless communications. Figure 5 shows TCF versus the normalized thickness of guiding layers h/λ calculated by equation (2.4). In Fig. 5a, the TCF value decreases with increasing ZnO film thickness. For ZnO/90AT Quartz, the TCF is found to be negative and varies from -13.77 to -47.44 ppm/°C for a ZnO normalized thickness variation in the range of 0.005 to 0.085; in comparison, the TCF of ZnO/90ST Quartz is close to 0 ppm/°C at $h/\lambda = 0.0216$. This is because thickness of the ZnO layer is enough to compensate for the high positive TCF of 90ST Quartz (40 ppm/°C). However, because of the small positive TCF of 90AT Quartz (0-1 ppm/°C), the high negative TCF of ZnO (-28 ppm/°C) makes the TCF of ZnO/90AT Quartz negative. In Fig. 5b, the TCF value increases with the increasing film thickness. For SiO₂/90ST Quartz, the TCF is found to be positive and varies from 8.0103 to 25.2037 ppm/°C for a SiO₂ normalized thickness variation in the range of 0.005 to 0.105; in comparison, the TCF of SiO₂/90AT Quartz

is close to 0 ppm/°C at $h/\lambda = 0.065$. This is because SiO₂ has a near-zero coefficient of thermal expansion, also resulting in a smaller TCF.

3.5. Mass sensitivity (S)

Figure 6 shows the mass sensitivity (calculated by Eq. (2.6)) as a function of h/λ for 90ST and 90AT Quartz substrates. The maximum value of the mass sensitivity is shown in Table 2. The sensitivity dispersion curves show similar trends, but the sensor with the ZnO guiding layer shows the maximum sensitivity nearly two times higher than that with the SiO₂ layer, and the corresponding thickness of ZnO is significantly smaller than that of SiO₂. The reason is explained as in the following.

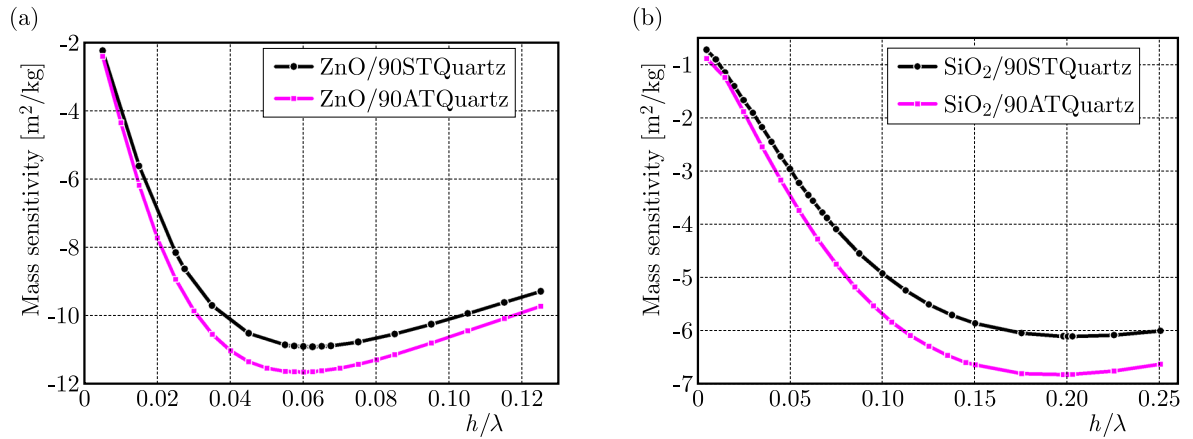


Fig. 6. Mass sensitivity as a function of normalized guiding thickness: (a) ZnO guiding layer, (b) SiO₂ guiding layer

Table 2. The maximum of mass sensitivity and its corresponding guiding thickness

Substrate	Guiding layer	Maximum of mass sensitivity [m ² /kg]	h/λ
90ST Quartz	ZnO	-10.9069	0.0625
	SiO ₂	-6.111	0.2025
90AT Quartz	ZnO	-11.641	0.0600
	SiO ₂	-6.831	0.1975

Figure 7 shows the relation between the x component of displacement and depth. When the thickness of ZnO equals 2.5 μm ($h_{\text{ZnO}}/\lambda = 0.0625$) at which the sensitivity of the ZnO/90ST Quartz reaches the maximum, almost all the acoustic energy is trapped in the ZnO guiding layer, whereas when SiO₂ takes the same value of thickness, the acoustic energy penetrates into the substrate deeply, so the corresponding sensitivity is lower. When the thickness of SiO₂ increases to the value of 8.1 μm ($h_{\text{SiO}_2}/\lambda = 0.2025$), almost all the acoustic energy is trapped in the SiO₂ guiding layer, so the sensitivity achieves the maximum. In Fig. 6, a further increase of the thickness decreases the sensitivity, because deeper penetration depth corresponds to weaker confinement of energy near the surface.

The above results are based on massless IDT electrodes. In practice, Au, Ni and Al are the common materials used for IDT. But they subject the SAW device to secondary effects such as a bulk acoustic wave and triple transit signals. Graphene, which is conductive and light, is expected to minimize the secondary effects when used as transducers (Sato, 2015). So, the advantages of the Love wave sensor with graphene IDT are explored. Table 3 gives the additional shifts in velocity δV and sensitivity δS achieved for graphene and Al electrodes with thickness

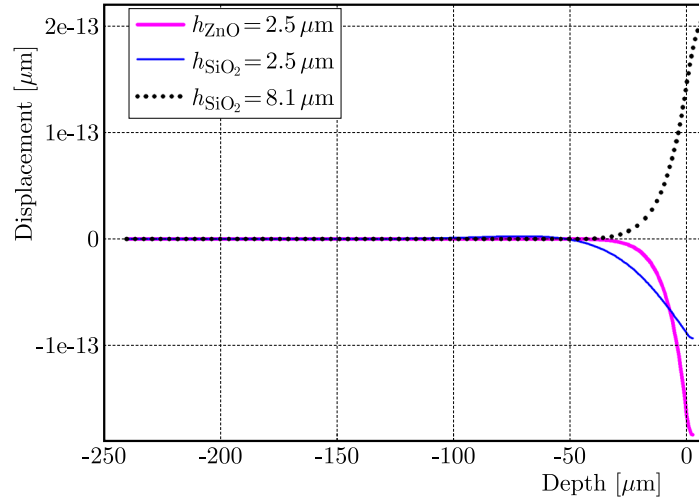


Fig. 7. The x component of displacement as a function of depth

of 60 nm when attached to the interface between ZnO ($h_{\text{ZnO}} = 2.5 \mu\text{m}$) and the substrate. It is shown the Love wave sensor employing the graphene electrode exhibits nearly one order of magnitude higher δS than that with Al electrode.

Table 3. The additional shifts in velocity and sensitivity due to graphene or Al electrode

Substrates	Electrodes	δV [m/s]	δS [m^2/kg]
90ST	Al	4.2	0.0594
	Graphene	57.4	0.8114
90AT	Al	4.4	0.0648
	Graphene	59.6	0.8776

4. Conclusions

The characteristics of the Love wave sensor based on SiO_2 or ZnO guiding layers overlaid on different cuts of quartz are systematically investigated. The combination of the guiding layer of ZnO and the substrate of 90ST or 90AT Quartz exhibits the purer Love mode and shows the maximum sensitivity nearly two times higher than that of the SiO_2 layer. The Love wave sensor with the ZnO/90ST Quartz structure exhibits the largest value of K^2 among the four combination structures and achieves $0 \text{ ppm}/^\circ\text{C}$ of TCF at $h_{\text{ZnO}}/\lambda = 0.0216$. If the sensor employs the graphene electrode as IDT, it will exhibit nearly one order of magnitude higher δS than that with Al electrode. The Love wave sensor with the 90ST Quartz substrate, ZnO guiding layer and graphene IDT is the optimal configuration for biosensing.

Acknowledgements

This work was supported by the National Natural Science Foundation of China (grant No. 11604025); and the Program of Science and Technology Development Plan of Jilin Province of China (grant No. 20200201249JC).

References

1. ANDERSON D.L., 1961, Elastic wave propagation in layered anisotropic media, *Journal of Geophysical Research*, **66**, 9, 2953-2963

2. FAN Y., JI X., 2018, A novel rotation speed measurement method based on surface acoustic wave, *Acoustical Physics*, **64**, 1, 122-128
3. FRANSSILA S., 2004, *Introduction to Microfabrication*, 4th ed., Wiley, Hoboken
4. FU Y.Q., LUO J.K., DU X.Y., FLEWITT A.J., LI Y., MARKX G.H., WALTON A.J., MILNE W.I., 2010, Recent developments on ZnO films for acoustic wave based bio-sensing and microfluidic applications: a review, *Sensors and Actuators B: Chemical*, **143**, 2, 606-619
5. JAKOBY B., BASTEMEIJER J., VELLEKOOP M.J., 2000, Temperature-compensated Love-wave sensors on quartz substrates, *Sensors and Actuators A: Physical*, **82**, 1-3, 83-88
6. JANDAS P.J., LUO J., QUAN A., QIU C., CAO W., FU C., FU Y., QUAN Q., 2020, Highly selective and label-free Love-mode surface acoustic wave biosensor for carcinoembryonic antigen detection using a self-assembled monolayer bioreceptor, *Applied Surface Science*, **518**, 15, 146061
7. KRISHNAMOORTHY S., ILIADIS A.A., 2008, Properties of high sensitivity ZnO surface acoustic wave sensors on SiO₂/(100)Si substrates, *Solid-State Electronics*, **52**, 11, 1710-1716
8. LUO J., LUO P., XIE M., DU K., ZHAO B., PAN F., FAN P., ZENG F., ZHANG D., ZHENG Z., LIANG G., 2013, A new type of glucose biosensor based on surface acoustic wave resonator using Mn-doped ZnO multilayer structure, *Biosensors and Bioelectronics*, **49**, 512-518
9. LUO J., QUAN A., FU C., LI H., 2017a, Shear-horizontal surface acoustic wave characteristics of a (110) ZnO/SiO₂/Si multilayer structure, *Journal of Alloys and Compounds*, **693**, 558-564
10. LUO J.T., QUAN A.J., LIANG G.X., ZHENG Z.H., RAMADAN S., FU C., FU Y.Q., 2017b, Love-mode surface acoustic wave devices based on multilayers of TeO₂/ZnO/Si(100) with high sensitivity and temperature stability, *Ultrason*, **75**, 63-70
11. MATATAGUI D., FONTECHA J., FERNÁNDEZ M.J., ALEIXANDRE M., GRÀCIA I., CANÉ C., HERRILLO M.C., 2011, Array of Love-wave sensors based on quartz/Novolac to detect CWA simulants, *Talanta*, **85**, 3, 1442-1447
12. MOREIRA F., EL HAKIKI M., SARRY F., LE BRIZOUAL L., ELMAZRIA O., ALNOT P., 2007, Numerical development of ZnO/quartz Love wave structure for gas contamination detection, *IEEE Sensors Journal*, **7**, 3, 336-341
13. POWELL D.A., KALANTAR-ZADEH K., WLODARSKI W., 2004, Numerical calculation of SAW sensitivity: application to ZnO/LiTaO₃ transducers, *Sensors and Actuators A: Physical*, **115**, 2-3, 456-461
14. SATO S., 2015, Graphene for nanoelectronics, *Japanese Journal of Applied Physics*, **54**, 4, 040102-1-040102-12
15. TANG Q.B., GUO Y.J., TANG Y.L., LONG G.D., WANG J.L., LI D.J., ZU X.T., MA J.Y., WANG L., TORUN H., FU Y.Q., 2019, Highly sensitive and selective Love mode surface acoustic wave ammonia sensor based on graphene oxides operated at room temperature, *Journal of Materials Science*, **54**, 11925-11935
16. TANG Y.L., LI Z.J., MA J.Y., GUO Y.J., FU Y.Q., ZU X.T., 2014, Ammonia gas sensors based on ZnO/SiO₂ bi-layer nanofilms on ST-cut quartz surface acoustic wave devices, *Sensors and Actuators B:Chemical*, **201**, 114-121
17. TURNER A.P.F., 2013, Biosensors: sense and sensibility, *Chemical Society Reviews*, **42**, 8, 3184-3196
18. WANG Z., CHEEKE J.D.N., JEN C.K., 1994, Sensitivity analysis for Love mode acoustic gravimetric sensors, *Applied Physics Letters*, **64**, 22, 2940-2942
19. ZADEH K.K., TRINCHI A., WLODARSKI W., HOLLAND A., 2002, A novel Love-mode device based on a ZnO/ST-cut quartz crystal structure for sensing applications, *Sensors and Actuators A: Physical*, **100**, 2-3, 135-143